CFTR-deficient pigs display alterations of bone microarchitecture and composition at birth

Julien Braux, Marie-Laure Jourdain, Christine Guillaume, Valérie Untereiner, Olivier Piot, Andrea Baehr, Nikolai Klymiuk, Nathalie Winter, Mustapha Berri, Dominique Buzoni-Gatel, et al.

Journal of Cystic Fibrosis 19 (2020) 466–475

Contents lists available at ScienceDirect

Journal of Cystic Fibrosis

journal homepage: www.elsevier.com/locate/jcf

Original Article

CFTR-deficient pigs display alterations of bone microarchitecture and composition at birth

Julien Braux[a], Marie-Laure Jourdain[a], Christine Guillaume[a], Valérie Untereiner[b], Olivier Piot[c], Andrea Baehr[d], Nikolai Klymiuk[d], Nathalie Winter[e], Mustapha Berri[e], Dominique Buzoni-Gatel[e], Ignaccio Caballero[e], Antoine Guillon[f], Mustapha Si-Tahar[f], Jacky Jacquot[a,*], Frédéric Velard[a,*]

[a] Université de Reims Champagne Ardenne, BIOS EA 4691, Biomatériaux et Inflammation en site osseux, SFR CAP-Santé (FED 4231), 1, Avenue du Maréchal Juin, 51097 Reims, France
[b] Université de Reims Champagne Ardenne (URCA), PICT Platform, Reims, 1, Avenue du Maréchal Juin, 51097 Reims, France
[c] Université de Reims Champagne-Ardenne, BioSpecT (Translational BioSpectroscopy) EA 7506, 1, Avenue du Maréchal Juin, 51097 Reims, France
[d] Institute of Molecular Animal Breeding and Biotechnology, Gene Center, Ludwig-Maximilians-Universitat Munchen, Hackerstrasse 27, 85764, Oberschleissheim, Germany
[e] INRA, UMR1282 ISP, Centre de recherches INRA Val de Loire, 37380, Nouzilly, France
[f] Inserm, Centre d'Etude des Pathologies Respiratoires, UMR1100/EA6305, 10 Boulevard Tonnellé, 37032, Tours, France

ARTICLE INFO

Article history:
Received 17 April 2019
Revised 7 October 2019
Accepted 22 October 2019
Available online 29 November 2019

Keywords:
Cystic fibrosis
Bone disease
Pigs
Cftr
Cortical bone
Trabecular bone
Femur

ABSTRACT

Background: The lack of cystic fibrosis transmembrane conductance regulator (CFTR) function causes cystic fibrosis (CF), predisposing to severe lung disease, reduced growth and osteopenia. Both reduced bone content and strength are increasingly recognized in infants with CF before the onset of significant lung disease, suggesting a developmental origin and a possible role in bone disease pathogenesis. The role of CFTR in bone metabolism is unclear and studies on humans are not feasible. Deletion of CFTR in pigs (*CFTR* $^{-/-}$ pigs) displays at birth severe malformations similar to humans in the intestine, respiratory tract, pancreas, liver, and male reproductive tract.

Methods: We compared bone parameters of *CFTR* $^{-/-}$ male and female pigs with those of their wild-type (WT) littermates at birth. Morphological and microstructural properties of femoral cortical and trabecular bone were evaluated using micro-computed tomography (μCT), and their chemical compositions were examined using Raman microspectroscopy.

Results: The integrity of the *CFTR* $^{-/-}$ bone was altered due to changes in its microstructure and chemical composition in both sexes. Low cortical thickness and high cortical porosity were found in *CFTR* $^{-/-}$ pigs compared to sex-matched WT littermates. Moreover, an increased chemical composition heterogeneity associated with higher carbonate/phosphate ratio and higher mineral crystallinity was found in *CFTR* $^{-/-}$ trabecular bone, but not in *CFTR* $^{-/-}$ cortical bone.

Conclusions: The loss of *CFTR* directly alters the bone composition and metabolism of newborn pigs. Based on these findings, we speculate that bone defects in patients with CF could be a primary, rather than a secondary consequence of inflammation and infection.

1. Introduction

Cystic fibrosis (CF) disease, which is caused by mutations of the CF transmembrane conductance regulator (*CFTR*) gene, is characterized by multiorgan deficiencies that begin early in life [1,2]. With the increasing life expectancy due to improvements in the treatment of the disease's pulmonary and gastrointestinal disorders, other CF complications and comorbidities have become more prevalent, such as diabetes and CF-related bone disease (CFBD) with 55–65% of affected patients being older than 45 [3–5]. Individuals with CF have low bone mineral density (BMD) [6–8] and increased fracture rate as early as adolescence, [9] which leads to

* Corresponding authors.
E-mail addresses: jacky.jacquot@inserm.fr (J. Jacquot), frederic.velard@univ-reims.fr (F. Velard).

https://doi.org/10.1016/j.jcf.2019.10.023

excessive kyphosis, thus weakening the thoracic skeletal architecture and resulting in an accelerated decline in lung function, ineffective cough and airway clearance [10–12].

The identification of bone composition and microarchitecture in patients with CF is a major determinant of bone density and fracture risk. Well done cross-sectional and longitudinal studies have indicated diminished bone accrual during the skeletal formative period of late childhood and adolescence [11,13,14]. A recent report showed a 9-fold higher fracture rate in young German CF adults compared to the age-matched reference population [15]. It is still unknown if the smaller stature in CF patients is a direct cause of loss of CFTR or a manifestation of nutritional deficiencies and inflammation [16]. Lower BMD gains were observed in infants with CF as early as the age of 6 with normal nutritional status, suggesting that CFBD may be due to a primary defect in bone metabolism [17].

CFTR protein was first discovered as being expressed during early development and was then identified in human bone cells [18], so CFTR deficiency may impact fetal tissues during in utero development. Cortical bone mass, comprising 85% of the skeleton, and bone microarchitecture are major determinants of bone strength and fracture risk in humans [18]. Skeletal homeostasis is maintained throughout life by the balance between bone-forming osteoblasts (which derive from mesenchymal cells) and bone-resorptive osteoclasts (which have hematopoietic origin) [19]. In patients with CF, we suggested a direct genetic component of CFBD with an abnormal elevation in receptor activator of NF-kB ligand (RANK-L) in osteoblasts bearing the F508del mutation in *Cftr* [20]. We recently reported that the CFTR potentiator ivacaftor improved BMD in G551D-bearing CF patients and argued for a link between CFTR activity and the function of osteoblasts [7] and osteoclasts precursors [21]. Several studies made on animal models (rats, mice and pigs) with CF shortly after birth revealed abnormalities in bone development [24–27] and tracheal cartilage with early airflow obstruction [27–31], suggesting the critical role of CFTR dysfunction. Several other species (ferret [32], zebrafish [33]) were used for this investigation on CF pathology.

The anatomy and physiology of pigs are similar to that of humans [22]. The *CFTR* $^{-/-}$ pig model develops both intestinal (meconium ileus, microcolon) and lung pathology, lesions in smooth muscle and cartilage rings resembling alterations observed in CF patients [23]. This emphasizes that CF pigs mimic the human condition to overcome several of the limitations found in CF mouse models. We recently targeted the porcine *CFTR* gene and generated *CFTR* $^{-/-}$ pigs which also display at birth severe malformations in the intestine, respiratory tract, pancreas, liver, and male reproductive tract [24,25]. These phenotypic abnormalities closely resemble both the human CF pathology as well as alterations observed in a previously published CF pig model generated by a different gene targeting strategy [26]. This new model provided us with an opportunity to ask whether *CFTR* $^{-/-}$ pigs (male and female) also manifest a defective bone microarchitecture and chemical composition at birth.

2. Methods

2.1. Animals

All experiments were conducted in accordance with the guidelines of the Institutional Animal Care and Use Committee at INRA. The protocol was approved by the "Comité d'Ethique en Expérimentation Animale Val de Loire" (n° 00028.01). *CFTR* $^{+/-}$ pigs were produced by replacing the exon 1 of the CFTR gene by a STOP box and a neo cassette using homologous recombination by BAC vectors as previously described [25]. Single male and female *CFTR*$^{+/-}$ transgenic pigs were moved to INRA, Nouzilly (France) and mated to generate wild-type (WT), *CFTR*$^{+/-}$ and *CFTR*$^{-/-}$ animals. Piglets were euthanized with an *i.v.* overdose of pentobarbital (Dolethal, Vétoquinol, France). A total of 17 WT and 23 *CFTR* $^{-/-}$ newborn piglets from 8 different litters were used in our experiments.

2.2. μCT evaluation

This study was conducted following the quantitative analysis of bone by micro-computed tomography recommendations from Campbell and Sophocleus [27]. We examined the pigs' femoral cortical and trabecular bones less than 24 h after birth using micro computed tomography (μCT, Skyscan 1076) scans with the following settings: tube voltage, 80 kV; tube current, 0.125 mA; and voxel size, 17,9 × 17,9 × 17,9 μm^3. Samples were isolated, fixed in ethanol (70% in Dulbecco's Phosphate Buffer Saline, Gibco), washed then stored in same ethanol solution at 4 °C. For scanning, samples were cleaned from surrounding soft tissue, rehydrated through an overnight storage in saline medium, then scanned directly in that solution. Three-dimensional (3D) images were rebuilt and analysed using respectively the NRecon GPU version and CTAn (Bruker) software programs. Bone mineral densities values were obtained using a standard regression line generated by converting the attenuation coefficient from scans of hydroxyapatite standards with known densities to mineral density (0.25 and 0.75 $g.cm^{-3}$). After 3D reconstruction, bone volumes were segmented using a global threshold of 0.373 g/cm^3 which was set using the mean density leading to the segment bone retrieved in scans after manual segmentation. The whole femoral bone was first studied to avoid bias due to the use of regions of interest. Common bone parameters were assessed (Femoral Length, Tissue volume (TV), Bone volume (BV), Percent bone volume (BV/TV), Tissue surface (TS), Bone surface (BS), Bone surface density (BS/TV), and Bone Mineral Density (BMD).

Then a 3.4-mm-wide region of interest centered on the middle of the femur was analysed to complete the cortical bone study (Fig. 1A, B). In cortical regions, we analysed the cortical total volume (Ct.TV), the cortical bone volume (Ct.BV), the bone volume density (Ct.BV/Ct.TV), the cortical mineral density (Ct.BMD), the cortical tissue surface (Ct.TS), the cortical bone surface (Ct.BS), the cortical bone surface density (Ct.TS/TV), the cortical thickness (Ct.Th), the cortical radius (Ct.Rd), and the ratio of cortical thickness / bone radius. The porosity of bones was assessed by calculating the porosity (defined as a connected assemblage of empty (black) voxels that is fully surrounded on all sides by solid (white) voxels) expressed as pores number, volume, surface and percentage of the volume of pores within the bone. X-rays 3D rebuilds that highlighed porosities were calculated on the samples presenting median values in terms of volume of pores.

For the trabecular bone, Tb.BV, Tb.TV, Tb.BV/Tb.TV, Tb.TS, Tb.BS, Tb.BS/Tb.TS trabecular number (Tb.N), trabecular thickness (Tb.Th), trabecular separation (Tb.Sp), trabecular pattern factor (Tb.Pf), and Tb.BMD were calculated while analysing a 2-mm-wide region of interest located 1 mm under the growth plate (Fig. 1A, C). A total of 23 newborn *CFTR* $^{-/-}$ piglets (14 males and 9 females) and 17 newborn WT piglets (8 males and 9 females) were subjected to µCT scan.

2.3. Raman imaging spectroscopy

The composition and distribution of organic and inorganic components of the cortical and trabecular bones were evaluated

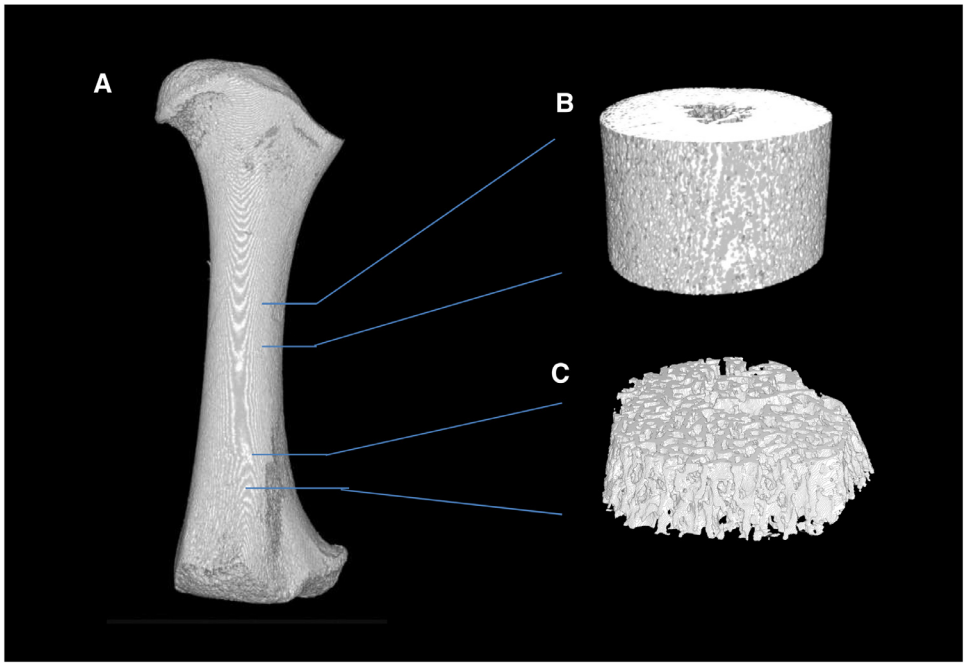

Fig. 1. Femoral bone regions of interest are: *A*) whole femoral bone, *B*) cortical bone was analyzed in a ROI centered on the femoral midshaft defined as the midpoint of the femoral bone, *C*) trabecular bone was analyzed at the distal femoral metaphysis, starting 1 mm away from the growth plate.

using Raman imaging spectroscopy. Raman provides quantitative information on the changes in the mineral and matrix composition as well as the nature and quantities of mineral constituents. Raman spectroscopy was chosen over infrared spectroscopy in this study as it has several inherent advantages such as minimal sample preparation, application to biological samples and potential in vivo implementation [28].

Raman images were recorded using a LabRam Aramis spectrometer (Horiba Scientific, Villeneuve d'Ascq, France) equipped with an Olympus microscope (model BX41) and a 100× long-working distance objective (Olympus, NA 0.9) for sample excitation and scattered light collection. The laser used for excitation was a diode emitting a radiation at 785 nm, near infrared excitation source, delivering around 13 mW to the sample. The Raman signal was dispersed using a 1200 lines/mm grating. For each bone sample (4 *CFTR* $^{-/-}$ and 3 WT piglets) subjected to Raman spectroscopy, twenty images were recorded in both cortical and trabecular areas of femurs. For each acquisition, the total exposure time was 60 s using 2 accumulations of 30 s. For any region of each sample, 20 spectra were combined to obtain an average spectrum. These were then averaged for all of the bones of each genotype to obtain an overall average. The spectra wavenumbers were detected on the fingerprint range (600–1800 cm^{-1}). Before analysis, raw Raman spectra need to be pre-processed. This was done with a home-made software using the Matlab environment (The MathWorks, Inc., Natick, Massachusetts). All spectra were first corrected for instrument response, and smoothed with a Savistsky-Golay function (second order polynomial, 7-point window length) to reduce noise. Afterwards, all spectra were baseline corrected with a polynomial function (order 2) and were vector-normalized in order to make the spectra comparable. An unsupervised processing method, principal component analysis (PCA), was performed on the pre-processed data to explore the spectral variability of the datasets. This method allows spectral data reduction replacing original and correlated variables by synthetic and uncorrelated variables called principal components (PCs). These PCs contain the total information and are arranged to explain the highest to lowest variance of the dataset. The results are presented using the scores of the most explained PCs. PC loadings are also useful to highlight the molecular origins of the spectral variability specific to a dataset. In this study, the mean spectrum of each group was subtracted from the individual spectra of the same group in order to remove redundant information, and PCA score plots were performed in the spectral range 1100–800 cm^{-1}.

Bone is composed of ~65 wt% mineral-non-stoichiometric hydroxyapatite ($Ca_{10}(PO_4)_6(OH)_2$), 10 wt% water, and 25 wt% organics. Organics mainly include type I collagen (~22.5 wt%), non-collagenous proteins (2.5–3.75 wt%), and lipids (1–10 wt%) [29]. In our Raman study, the intensities of the following vibration peaks were measured: phosphate $\upsilon 1$ at ~958 cm-1 (PO_4^{3-} symmetric stretching), carbonate $\upsilon 1$ at ~1071 cm^{-1} (CO_3^{2-} symmetric stretching), CH_2 wagging at ~1450 cm^{-1} (C–H bending), amide I around 1667 cm-1 (mainly C=O stretching of the peptide bonds), amide III at ~1243 cm^{-1} (in-phase combination of the N–H bending and C–N stretching). The width of phosphate $\upsilon 1$ at ~958 cm^{-1} was also measured for both cortical and trabecular bones. Three bone compositional parameters were examined: i/ the mineral-to-matrix ratio estimated using the integrated intensities under the baselined peak from 915 to 1215 cm^{-1} over the amide I area (1596–1720 cm^{-1}), ii/ the carbonate-to-phosphate ratio calculated from the ratio of integrated intensities 850–895 cm^{-1}/915–1215 cm^{-1}, and iii/ the mineral crystallinity determined by the inverse of the phosphate 958 cm^{-1} bandwidth. It was reported by a number of researchers that the bandwidth of the $PO_4^{3-}\upsilon_1$ peak decreases as the mineral crystallinity improves (increase in the crystal size and/or atomic ordering) [30].

2.4. Statistical analyses

The effect of genotype was statistically assessed. Morphological measures of *CFTR* $^{-/-}$ and WT bones were compared using the Wilcoxon signed rank test (paired samples) where pigs were compared to their siblings. Measurements obtained from the Raman analysis were evaluated using analysis of variance (one-way nested ANOVA). *P*-values smaller than 0.05 were considered significant.

Table 1
Piglet characteristics and macrostructural indexes.

	n	Body Weight (kg - mean ± SD)	Femur Length (mm - mean ± SD)	Femur Volume (cm3 - mean ± SD)	Femur Bone Volume (cm3 - mean ± SD)	% Bone Volume (mean ± SD)
			Whole Bone			
WT						
Male	8	1.098 ± 0.186	40.56 ± 2.38	1.94 ± 0.40	1.03 ± 0.29	53.32 ± 6.04
Female	9	1.182 ± 0.293	41.23 ± 2.91*	2.11 ± 0.46#	1.15 ± 0.29§	54.34 ± 4.90μ
CFTR$^{-/-}$						
Male	14	1.185 ± 0.339	40.52 ± 4.34	1.92 ± 0.48	0.98 ± 0.22	51.35 ± 7.24
Female	9	1.170 ± 0.281	39.50 ± 2.10*	1.86 ± 0.51#	0.95 ± 0.34§	50.49 ± 6.41μ

Wilcoxon signed rank tests; *, #, §, μ means statistically different (respectively $p = 0{,}029$, $p = 0{,}040$, $p = 0{,}010$ and $p = 0{,}048$).

3. Results

3.1. Femoral bone volume was reduced in CFTR KO piglets

At birth, the whole-body weight of 23 *CFTR* $^{-/-}$ and 17 WT newborn pigs was similar whatever the sex and genotype (Table 1). To determine whether *CFTR* played a role in bone mass, we first compared femur length and femoral volume of WT and *CFTR* $^{-/-}$ pigs (Table 1). Both femur length and femoral volume were significantly reduced in *CFTR* $^{-/-}$ female pigs compared to their respective WT littermates (39.50 mm ± 2.10 vs 41.23 mm ± 2.91 and 1.86 ± 0.51 cm^3 vs 2.11 ± 0.46 cm^3, respectively).

CFTR $^{-/-}$ female pigs had significantly reduced femoral bone volume in comparison to WT female pigs (reduced 17%, $p < 0.05$). Femoral bone volume was also reduced in male *CFTR* $^{-/-}$ pigs, but this did not reach statistical significance. Since the percentage of bone volume (femur bone volume / femur volume) was still reduced in *CFTR*-/- pigs, the reduction of femoral bone volume observed in *CFTR* -/- pigs could not be explained only by the shorter length and/or circumference of the femur (Table 1).

3.2. Cortical bone mass was reduced and intracortical porosity enhanced in CFTR KO piglets

Comparisons of cortical bone representative 3-D images between WT and *CFTR* $^{-/-}$ pigs were obtained as shown in the Figs. 1A, B and depicted in Fig. 2A. The cortical mineral density and cortical thickness/radius were lower in *CFTR* $^{-/-}$ male and female pigs compared to sex-matched WT littermates (Fig. 2B, C). We next assessed whether the loss of *CFTR* affected the cortical porosity, *via* μCT-based analyses. Views of representative 3D images of

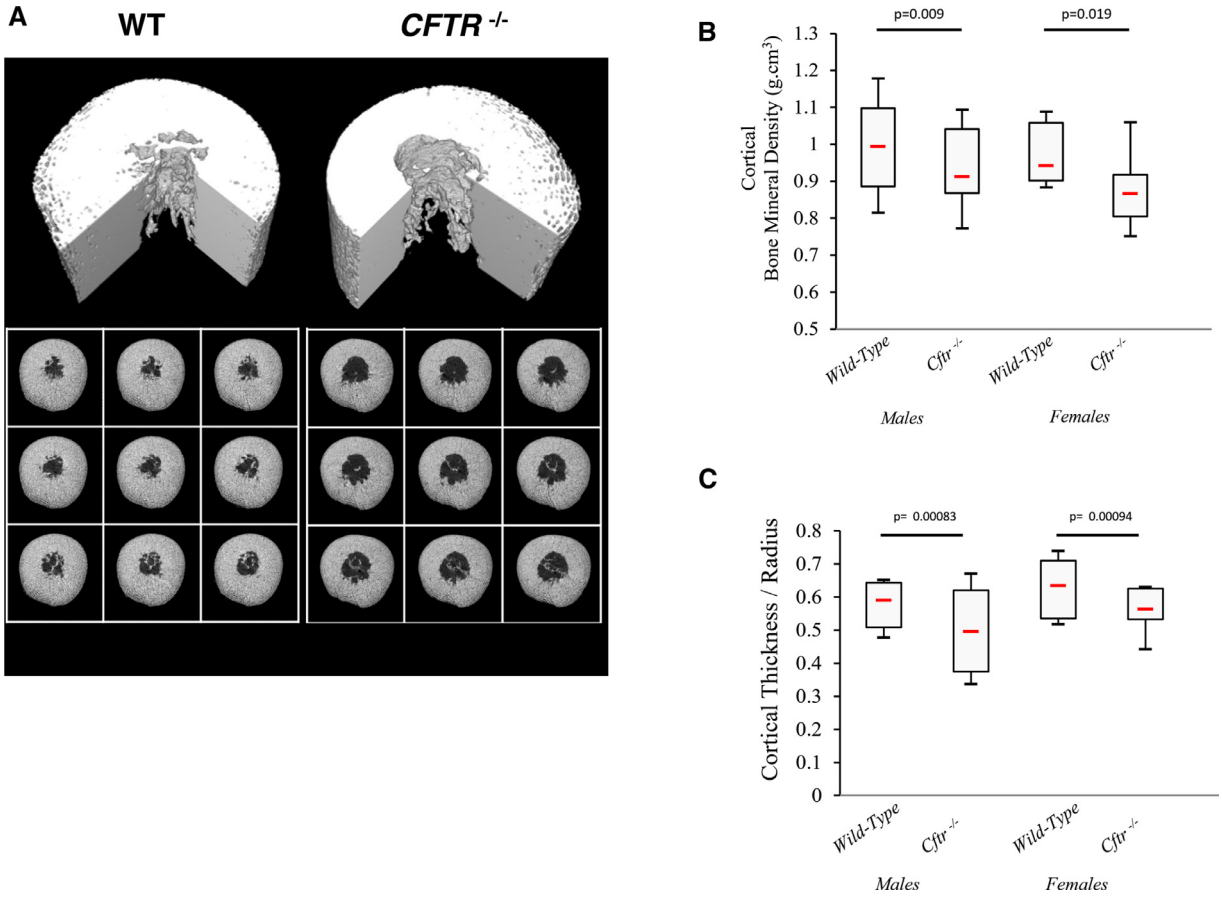

Fig. 2. Representative 3-D images of femoral cortical bone (*A*), cortical mineral density (*B*), and cortical thickness (*C*) of WT and *CFTR* $^{-/-}$ pigs.

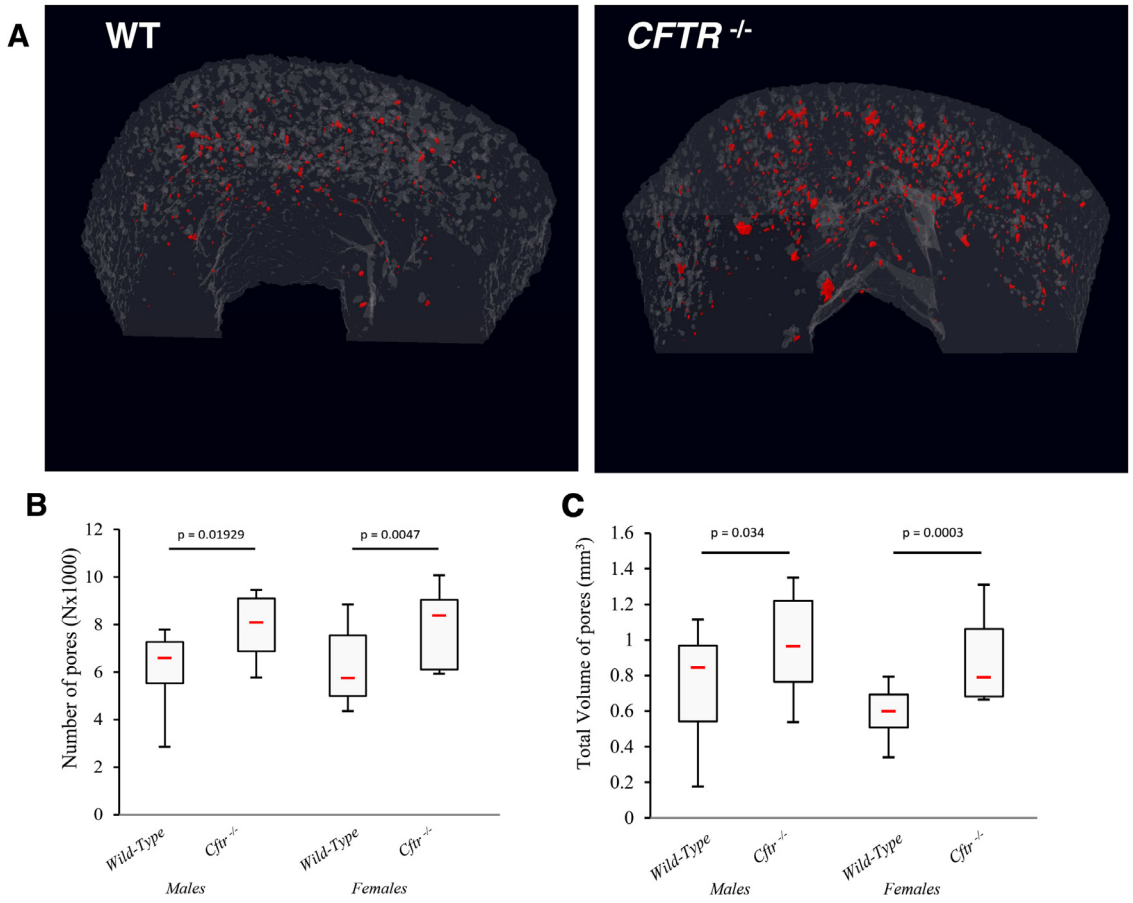

Fig. 3. Representative 3-D images of femoral cortical bone (*A*), number of pores (*B*) and total volume of pores (*C*) of WT and *CFTR* $^{-/-}$ pigs.

cortical bone sections from *CFTR* $^{-/-}$ and WT pigs were arranged with the cortical porosity distribution area highlighted in red (Fig. 3A, see video in supplementary data). We observed increases in both number and total volume of pores in *CFTR* $^{-/-}$ pigs compared to sex-matched WT littermates (Fig. 3B, C). Averages of 14% and 32% rise, respectively in male and female cortical porosities, were assessed in *CFTR* $^{-/-}$ pigs compared to their WT littermates.

3.3. Loss of CFTR did not reduce trabecular bone mass

Comparisons of trabecular bone parameters between groups based on gender were reported in Fig. 4A–H. Views of representative 3D images of trabecular bone sections from *CFTR* $^{-/-}$ and WT pigs were obtained as shown in the Fig. 1A-C and depicted in Fig. 4A. As observed in cortical bone, the trabecular BMD was lower in *CFTR* $^{-/-}$ male and female pigs compared to sex-matched WT littermates (Fig. 4B). However, trabecular bone volume was similar and even slightly increased in *CFTR* $^{-/-}$ male pigs compared to sex-matched WT littermates (Fig. 4C). The increased trabecular bone volume in *CFTR* $^{-/-}$ femurs was due to significant contributions:increased trabecular thickness and trabecular number (Fig. 4D, E).

We noticed a reduced trabecular pattern factor (Tb.Pf) (that meant more connected trabecular lattices) in *CFTR* $^{-/-}$ male pigs compared to WT littermates (Fig. 4F). If no difference could be revealed in the repartition of the trabecular thickness, a shift was highlighted in the repartition of trabecular separation (Fig. 4G, H). More precisely, a shift was observed in the distributions of the means of Trabecular Separation Ranges. Wild type samples tended to present less low trabecular separation distances (inferior to 268.5 µm) and more wide trabecular separation distances (more than 268.5 µm).

3.4. Both mineral-to-matrix ratio and mineral crystallinity had increased in trabecular bone but not in cortical bone of CFTR KO piglets

After determining through μCT scans that cortical and trabecular microstructures were altered in *CFTR* $^{-/-}$ pigs compared to sex-matched WT littermates, Raman spectroscopic measurements were performed to analyze the chemical composition of the cortical and trabecular bone of *CFTR* $^{-/-}$ pigs compared to WT. A typical Raman spectrum for cortical bone is shown in Fig. 5A. The profile of spectra from *CFTR* $^{-/-}$ and WT pigs was very similar in the whole spectral range.

Nevertheless, an unsupervised principle component analysis (PCA) was used and allowed to classify the spectra according to the piglets' two genotypes. PCA score plot of the cortical bone Raman spectra is shown (Fig. 5B). The two first principal components, PC1 (79.8%) and PC2 (9.4%) carrying the highest explained variance, were used to separate the two genotypes in spectral range 800–1100 cm^{-1}. We observed that *CFTR* $^{-/-}$ pigs exhibited more heterogeneity compared to WT. In each group, the number of female and male piglets was equivalent. The separation of two groups was based on the piglets' genotype and not on their gender (data not shown). To explain that discrimination between *CFTR* $^{-/-}$ and WT pigs, the loadings (PCs) were used, and showed differences in mineral components of cortical bone mainly associated to PO_4^{3-} (Fig. 5C).

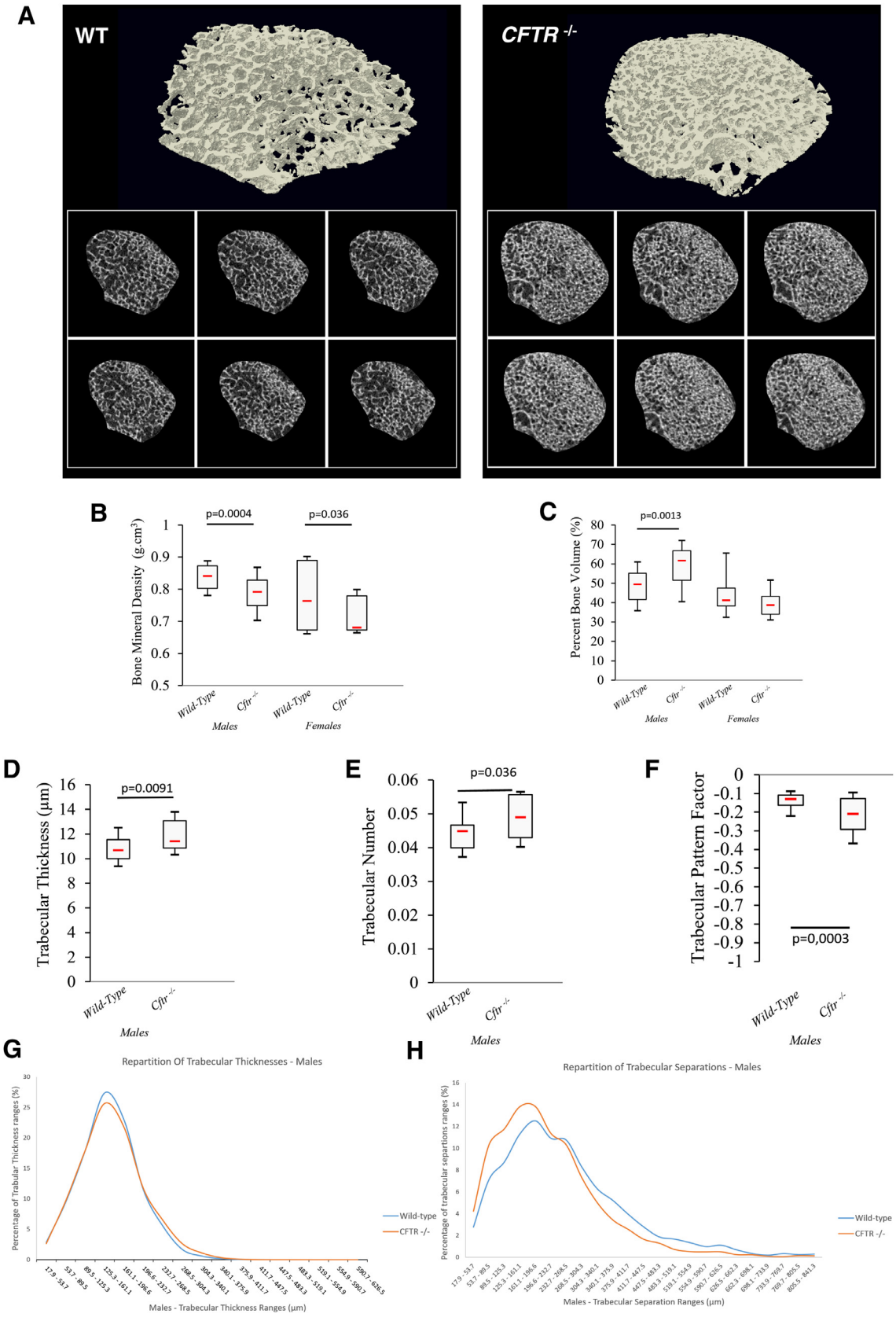

Fig. 4. Representative 3-D images of male femoral trabecular bone (A), trabecular mineral density (B), percent trabecular volume (C), trabecular thickness (D), trabecular number (E), trabecular pattern factor (F), and repartition of the mean percentages of each trabecular thickness ranges and separations retrieved in samples (G, H) of WT and *CFTR* -/- pigs.

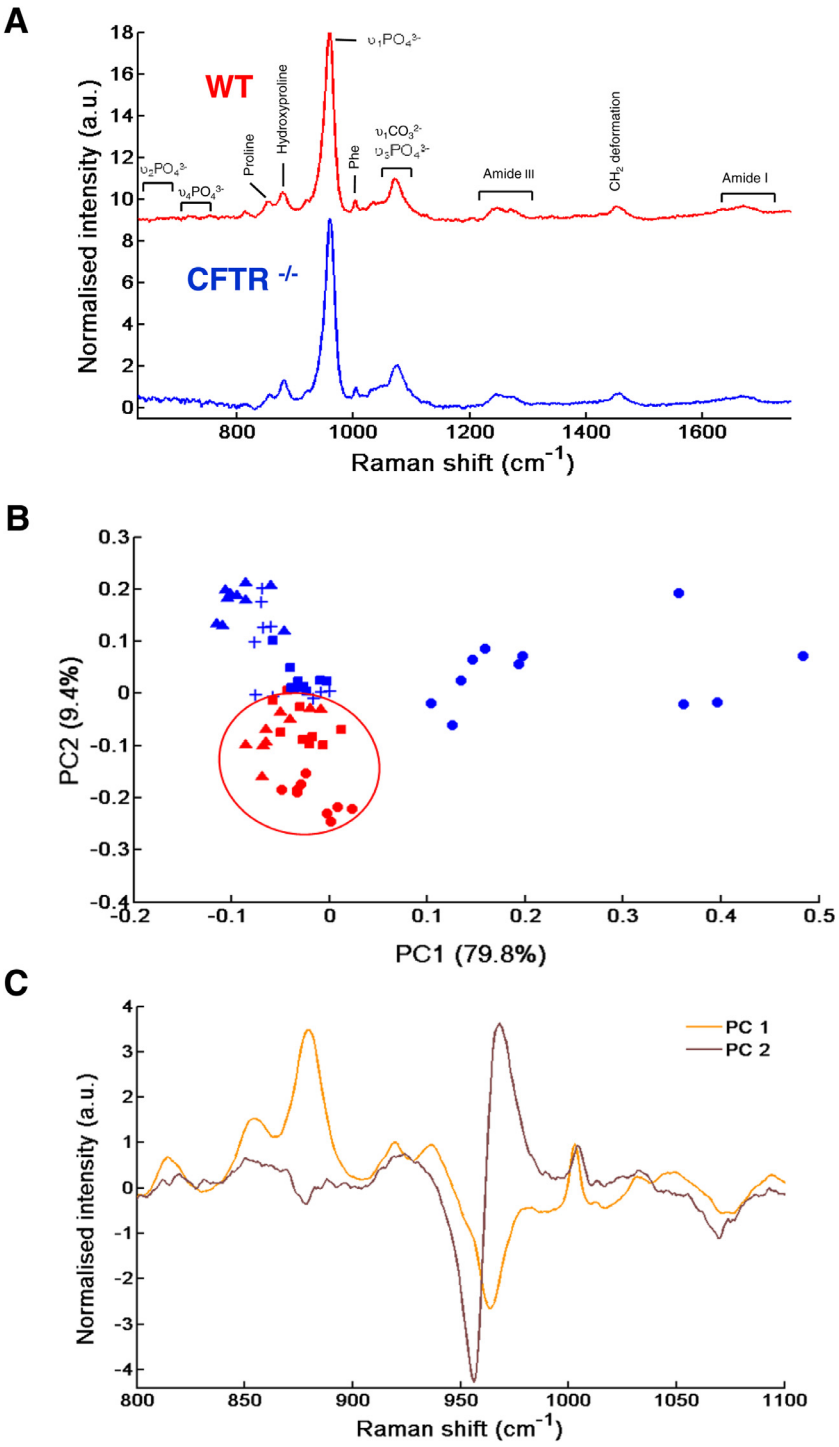

Fig. 5. Typical Raman spectrum of cortical bone from the WT (red line) and *CFTR* $^{-/-}$ (blue line) pigs. Major bone mineral and matrix band positions and associated spectral regions are marked (*A*). PCA score plot (PC1 vs PC2) with WT (red points) and *CFTR* $^{-/-}$ (blue points) pigs (*B*). Loadings of PC1 (orange curve) and PC2 (brown curve) (*C*). PCA and loadings were calculated in the spectral range 800–1100 cm-1. Each symbol/color couple represents an independent animal. (For interpretation of the references to color in this figure legend, the reader is referred to the web version of this article.)

A typical Raman spectrum for trabecular bone is shown in Fig. 6A. The spectral profiles between *CFTR* $^{-/-}$ and WT pigs mainly showed differences in the regions of amide III and CO_3^{2-} bands. PCA score plots were performed on spectra extracted from trabecular bone in two genotypes. The first two principal components PC1 and PC2 respectively carried 55.3% and 18.7% of total variance (Fig. 6B). The score plots showed a separation of *CFTR* $^{-/-}$ and WT pigs according to the PC1 in the spectral range 800–1100 cm^{-1}, as well as differences in mineral components associated to CO_3^{2-} (type-B carbonate) and phosphate groups (PO_4^{3-}) (Fig. 6C).

In addition to this multivariate processing by PCA, spectral data were submitted to ratiometric analyses. The mean values in the phosphate υ1/amide I ratio, type-B carbonate/ phosphate υ1ratio, and $1/PO_4^{3-}$ were calculated in both cortical and

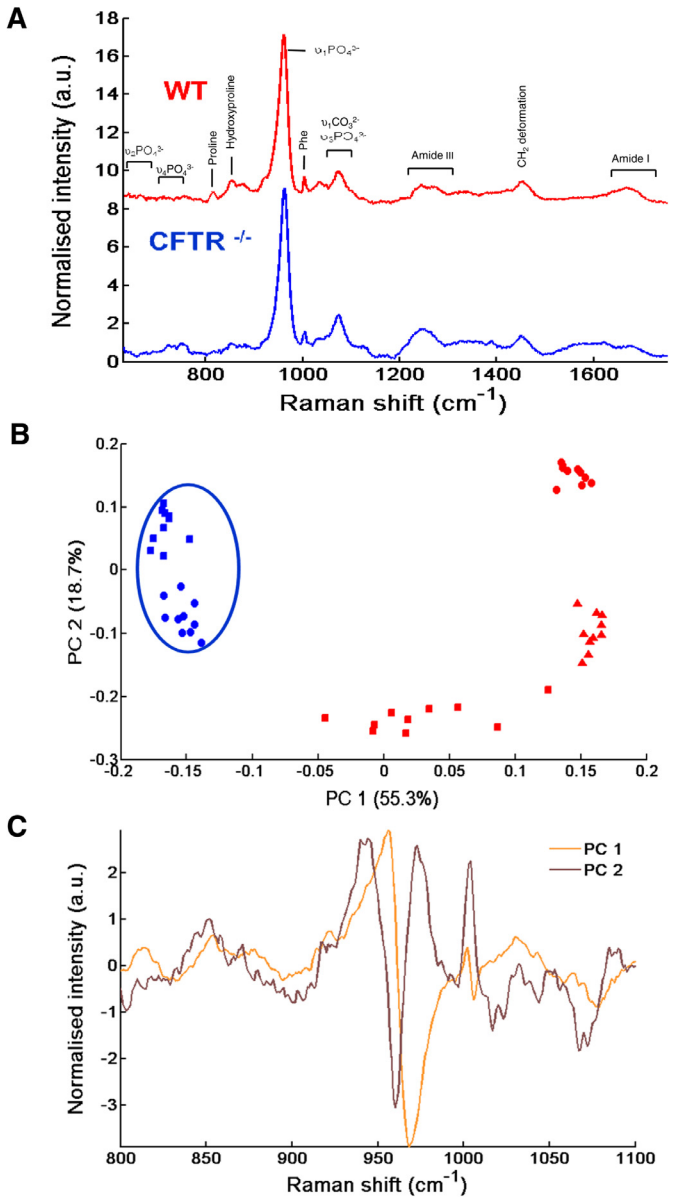

Fig. 6. Typical Raman spectrum of trabecular bone from the WT (red line) and *CFTR* $^{-/-}$ (blue line) pigs. Major bone mineral and matrix band positions and associated spectral regions are marked (*A*). PCA score plot (PC1 vs PC2) with WT (red points) and *CFTR* $^{-/-}$ (blue points) pigs (*B*). Loadings of PC1 (orange curve) and PC2 (brown curve) (*C*). PCA and loadings were calculated in the spectral range 800–1100 cm^{-1}. Each symbol/color couple represents an independent animal.

trabecular bones for each genotype (Table 2). A marked increase in the mineral/matrix ratio, the type-B carbonate substitution and the mineral crystallinity were observed in trabecular bone of *CFTR* $^{-/-}$ pigs compared to WT, but not found in cortical bone.

4. Discussion

Cortical bone composition and density are key determinants of bone strength and fracture risk in humans [18]. Recent studies reported an elevated fracture rate in CF patients [5,12,31] in relation with macroscopic bone architecture [32], and others described deficits in trabecular and cortical bone as well as strength in prepubertal children, adolescents and adults with CF [8,33–35]. People with CF have several risk factors to develop low bone mass and density including chronic lung inflammation, pancreatic insufficiency, malnutrition, delayed puberty, glucocorticoid use, and possibly *CFTR* dysfunction itself [3,11]. Therefore, it is necessary to discriminate between the clinical disease's multiple contributions and the intrinsic defect due to *CFTR* deficiency. At birth, lungs of CF pigs lack inflammation, but with time, they spontaneously develop infection, inflammation and remodeling [36]. To address the consequence of *CFTR* deficiency on bone microarchitecture, we compared bone parameters of *CFTR* $^{-/-}$ pigs to WT littermates at birth. Our data prove that *CFTR* is fundamental to maintain the correct chemical composition and microarchitecture of bone.

Several hypotheses emerged from our study regarding the function of *CFTR* in the bone metabolism. Our data demonstrate that a defective bone health is readily apparent in *CFTR* $^{-/-}$ pigs at birth. The length and bone volume of their femurs were reduced compared to WT pigs in females. Interestingly, Rogan et al. also demonstrated that CF piglets had reduced humeral length and bone mineral content [37]. In our study, we evidenced an altered bone microarchitecture in *CFTR* $^{-/-}$ pigs. Our µCT analysis of the bone architecture and mineral density reveals that *CFTR* deficiency alters cortical bone structure and reduces cortical and trabecular BMD. Low cortical thickness and high cortical porosity were found in *CFTR* $^{-/-}$ pigs. In contrast, trabecular bone volume was not altered in these pigs. In our study, we evaluated averages of 14% and 32% rise in porosity of *CFTR* $^{-/-}$ male and female pigs compared to sex-matched WT littermates. Elevated porosity is well known to diminish bone resistance against fracture by increasing the velocity of crack propagation [38,39]. The identification of mechanisms leading to enhanced porosity is likely to improve our understanding of the pathogenesis of CFBD.

Prior investigations have revealed that bone cortical thinning and increased porosity occur when the rate of bone remodeling is modified [40]. A possible altered bone remodeling of the *CFTR* $^{-/-}$ pigs is suggested by changes in the bones' chemical composition. Our Raman analysis of the *CFTR* $^{-/-}$ femurs indicated that, compared with WT pigs', their cortical bone was different in mineral components associated to CO_3^{2-} (type-B carbonate), and their trabecular bone was different in mineral components associated to CO_3^{2-} (type-B carbonate) and phosphate groups (PO_4^{3-}). In addition, at the trabecular level, carbonate substitutes for phosphate ions in bone (type-B carbonate) demonstrated that the phosphate environment of the mineral was distorted with an increased mineral/matrix ratio and elevated mineral crystallinity in *CFTR* $^{-/-}$ trabecular bone, all indicative of disrupted bone remodeling.

Table 2
The Phosphate $\upsilon 1$/Amide I Ratio, Type-B Carbonate/Phosphate $\upsilon 1$ratio and $1\upsilon/PO_4^{3-}$ in Trabecular and Cortical Bone in *CFTR* $^{-/-}$ and WT Pigs.

	Trabecular bone		Cortical bone	
Genotype WT	CFTR$^{-/-}$	WT	CFTR$^{-/-}$	WT
$\upsilon 1PO_4^{3-}$/amide I	26.57 ± 8.33*	0.22 ± 0.04	0.044 ± 0.009	0.061 ± 0.045
($CO_3^{2-}/\upsilon 1PO_4^{3-}$)	21.40 ± 9.33*	0.20 ± 0.01	0.205 ± 0.031	0.205 ± 0.031
$1/\upsilon 1PO_4^{3-}$ (x 10^{+3})	0.957 ± 0.336*	0.625 ± 0.208	0.600 ± 0.295	0.608 ± 0.283

Values are mean ± SEM. $n = 4$
* significantly different to WT ($p < 0.01$).

Our study supplements the multiple studies on CF mice and rats, which have identified reductions in cortical bone mass attributed to the loss of *CFTR* [41–44]. Our laboratory [45] and others [46,47] previously issued studies suggesting evidence of direct dependence on bone growth due to *CFTR*, we indeed reported that interventions to improve *CFTR* function in the F508del-*CFTR* mouse [48] and in CF patients bearing the G551D-mutation in *CFTR* resulted in enhanced bone density [7].

4.1. Limitations

Our data bears advantages and limitations. First, we used an animal model that was described to recapitulate human CF. Second, we hypothesized that a pig's bone was more similar to that of a human's than a mouse's [50]. Third, we were capable of eliminating secondary consequences of the disease by studying newborn pigs. As we did not address the role of bone *CFTR*, we were not able to exclude the possibility that *CFTR* gene in bone cells contributed to the phenotypes we observed.

We do not yet have a mechanism identified for the low cortical bone thickness and enhanced cortical porosity in *CFTR* $^{-/-}$ pigs at birth, but we suspect the phenotype may be dependent upon the altered osteoblastic activity and differentiation. Genetic studies confirmed that activating the canonical WNT signaling increased bone formation in mice by promoting osteoblast differentiation and indirectly inhibiting bone resorption, thus reducing osteoclastogenesis mainly by osteoprotegerin (OPG) regulation [19,49]. *CFTR* was shown to positively regulate WNT/β-catenin pathway in multiple cell types [51,52]. A decrease in canonical WNT signaling was reported in *CFTR* $^{-/-}$ rat osteoblasts [46], as well as a decreased WNT/β-catenin in F508del-*CFTR* mice signaling mediated reduced osteoblast differentiation and function [53]. A direct effect of canonical WNT signaling of osteoblasts on osteoclastogenesis was proposed, as mice lacking WNT16 in osteoblasts were characterized by a reduced cortical thickness and high cortical bone porosity while their trabecular bone remained unaffected [54].

In F508del-*CFTR* human osteoblasts, we recently reported an overexpression of receptor activator of nuclear factor kappa-B ligand (RANKL) and high membranous RANKL localization coupled with a reduced OPG production which could be reversed with *CFTR* activators [20]. That situation may reduce bone formation and worsen bone resorption through the activation of osteoclasts leading to low cortical bone mass in people with CF. Further molecular studies are needed to determine which of the signaling pathways may have contributed to the low cortical bone mass and high bone cortical porosity

5. Conclusion

We provide evidence that loss of *CFTR* alters bone chemical composition and microarchitecture in pigs at birth. This might indicate that bone defects in people with cystic fibrosis are likely primary, regardless of significant clinical confounders such as inflammation and infection from the start of life. The lower cortical bone mass in our study's *CFTR* $^{-/-}$ pigs and present in children and adolescents with CF [8] suggests that the use of *CFTR* potentiators and correctors might benefit people with CF bone disease as far as their skeletal health is concerned.

Declaration of Competing Interest

All authors report no conflicts of interest in this work.

Acknowledgments

This study was supported in part by the French Association Vaincre la Mucoviscidose, grants RF20130500925 and RF 20170501938. The authors thank Dr. Marjorie Cantener for correcting the manuscript.

Supplementary materials

Supplementary material associated with this article can be found, in the online version, at doi:10.1016/j.jcf.2019.10.023.

References

[1] Riordan JR, Rommens JM, Kerem B, et al. Identification of the cystic fibrosis gene: cloning and characterization of complementary DNA [published erratum appears in Science 1989 sep 29;245(4925):1437]. Science 1989;245:1066–73.
[2] Stoltz DA, Meyerholz DK, Welsh MJ. Origins of cystic fibrosis lung disease. N Engl J Med 2015;372:351–62.
[3] Jacquot J, Delion M, Gangloff S, et al. Bone disease in cystic fibrosis: new pathogenic insights opening novel therapies. Osteoporos Int 2016;27:1401–12.
[4] Plant BJ, Goss CH, Plant WD, et al. Management of comorbidities in older patients with cystic fibrosis. Lancet Respir Med 2013;1:164–74.
[5] Putman MS, Milliren CE, Derrico N, et al. Compromised bone microarchitecture and estimated bone strength in young adults with cystic fibrosis. J Clin Endocrinol Metab 2014;99:3399–407.
[6] Aris RM, Merkel PA, Bachrach LK, et al. Guide to bone health and disease in cystic fibrosis. J Clin Endocrinol Metab 2005;90:1888–96.
[7] Sermet-Gaudelus I, Delion M, Durieu I, et al. Bone demineralization is improved by ivacaftor in patients with cystic fibrosis carrying the p.Gly551Asp mutation. J Cyst Fibros 2016;15:e67–9.
[8] Kelly A, Schall J, Stallings VA, et al. Trabecular and cortical bone deficits are present in children and adolescents with cystic fibrosis. Bone 2016;90:7–14.
[9] Buntain HM, Greer RM, Schluter PJ, et al. Bone mineral density in Australian children, adolescents and adults with cystic fibrosis: a controlled cross sectional study. Thorax 2004;59:149–55.
[10] Paccou J, Zeboulon N, Combescure C, et al. The prevalence of osteoporosis, osteopenia, and fractures among adults with cystic fibrosis: a systematic literature review with meta-analysis. Calcif Tissue Int 2010;86:1–7.
[11] Sermet-Gaudelus I, Castanet M, Retsch-Bogart G, et al. Update on cystic fibrosis-related bone disease: a special focus on children. Paediatr Respir Rev 2009;10:134–42.
[12] Aris RM, Renner JB, Winders AD, et al. Increased rate of fractures and severe kyphosis: sequelae of living into adulthood with cystic fibrosis. Ann Intern Med 1998;128:186–93.
[13] Buntain HM, Schluter PJ, Bell SC, et al. Controlled longitudinal study of bone mass accrual in children and adolescents with cystic fibrosis. Thorax 2006;61:146–54.
[14] Sparks AA, McGee SJ, Boone CE, et al. 'Old' bones in young bodies: the tale of cystic fibrosis. Curr Opin Endocrinol Diabetes Obes 2009;16:407–14.
[15] Stahl M, Holfelder C, Kneppo C, et al. Multiple prevalent fractures in relation to macroscopic bone architecture in patients with cystic fibrosis. J Cyst Fibros 2016.
[16] Bournez M, Bellis G, Huet F. Growth during puberty in cystic fibrosis: a retrospective evaluation of a French cohort. Arch Dis Child 2012;97:714–20.
[17] Sermet-Gaudelus I, Souberbielle JC, Ruiz JC, et al. Low bone mineral density in young children with cystic fibrosis. Am J Respir Crit Care Med 2007;175:951–7.
[18] Zebaze RM, Ghasem-Zadeh A, Bohte A, et al. Intracortical remodelling and porosity in the distal radius and post-mortem femurs of women: a cross-sectional study. Lancet 2010;375:1729–36.
[19] Baron R, Kneissel M. WNT signaling in bone homeostasis and disease: from human mutations to treatments. Nat Med 2013;19:179–92.
[20] Delion M, Braux J, Jourdain ML, et al. Overexpression of RANKL in osteoblasts: a possible mechanism of susceptibility to bone disease in cystic fibrosis. J Pathol 2016;240:50–60.
[21] Velard F, Jourdain ML, Abdallah D, et al. Overexpression of RANK and M-CSFR in Monocytes of G551D-Bearing patients with cystic fibrosis. Am J Respir Crit Care Med 2018;198:968–70.
[22] Meyerholz DK. Lessons learned from the cystic fibrosis pig. Theriogenology 2016;86:427–32.
[23] Meyerholz DK, Stoltz DA, Namati E, et al. Loss of cystic fibrosis transmembrane conductance regulator function produces abnormalities in tracheal development in neonatal pigs and young children. Am J Respir Crit Care Med 2010;182:1251–61.
[24] Guillon A, Chevaleyre C, Barc C, et al. Computed tomography (CT) scanning facilitates early identification of neonatal cystic fibrosis piglets. PLoS ONE 2015;10:e0143459.
[25] Klymiuk N, Mundhenk L, Kraehe K, et al. Sequential targeting of CFTR by BAC vectors generates a novel pig model of cystic fibrosis. J Mol Med (Berl) 2012;90:597–608.
[26] Rogers CS, Stoltz DA, Meyerholz DK, et al. Disruption of the CFTR gene produces a model of cystic fibrosis in newborn pigs. Science 2008;321:1837–41.

[27] Campbell GM, Sophocleous A. Quantitative analysis of bone and soft tissue by micro-computed tomography: applications to ex vivo and in vivo studies. Bonekey Rep 2014;3:564.
[28] Mandair GS, Morris MD. Contributions of Raman spectroscopy to the understanding of bone strength. Bonekey Rep 2015;4:620.
[29] Goldberg M, Boskey AL. Lipids and biomineralizations. Prog Histochem Cytochem 1996;31:1–187.
[30] Akkus O, Polyakova-Akkus A, Adar F, et al. Aging of microstructural compartments in human compact bone. J Bone Miner Res 2003;18:1012–19.
[31] Haworth CS, Freemont AJ, Webb AK, et al. Hip fracture and bone histomorphometry in a young adult with cystic fibrosis. Eur Respir J 1999;14:478–9.
[32] Stahl M, Holfelder C, Kneppo C, et al. Multiple prevalent fractures in relation to macroscopic bone architecture in patients with cystic fibrosis. J Cyst Fibros 2018;17:114–20.
[33] O'Brien CE, Com G, Fowlkes J, et al. Peripheral quantitative computed tomography detects differences at the radius in prepubertal children with cystic fibrosis compared to healthy controls. PLoS ONE 2018;13:e0191013.
[34] Kelly A, Schall JI, Stallings VA, et al. Deficits in bone mineral content in children and adolescents with cystic fibrosis are related to height deficits. J Clin Densitom 2008;11:581–9.
[35] Nishiyama KK, Agarwal S, Kepley A, et al. Adults with cystic fibrosis have deficits in bone structure and strength at the distal tibia despite similar size and measuring standard and relative sites. Bone 2018;107:181–7.
[36] Stoltz DA, Meyerholz DK, Pezzulo AA, et al. Cystic fibrosis pigs develop lung disease and exhibit defective bacterial eradication at birth. Sci Transl Med 2010;2:29ra31.
[37] Rogan MP, Reznikov LR, Pezzulo AA, et al. Pigs and humans with cystic fibrosis have reduced insulin-like growth factor 1 (IGF1) levels at birth. Proc Natl Acad Sci U S A 2010;107:20571–5.
[38] Carriero A, Doube M, Vogt M, et al. Altered lacunar and vascular porosity in osteogenesis imperfecta mouse bone as revealed by synchrotron tomography contributes to bone fragility. Bone 2014;61:116–24.
[39] Carriero A, Zimmermann EA, Paluszny A, et al. How tough is brittle bone? Investigating osteogenesis imperfecta in mouse bone. J Bone Miner Res 2014;29:1392–401.
[40] Shigdel R, Osima M, Ahmed LA, et al. Bone turnover markers are associated with higher cortical porosity, thinner cortices, and larger size of the proximal femur and non-vertebral fractures. Bone 2015;81:1–6.
[41] Dif F, Marty C, Baudoin C, et al. Severe osteopenia in CFTR-null mice. Bone 2004;35:595–603.
[42] Le Henaff C, Gimenez A, Hay E, et al. The F508del mutation in cystic fibrosis transmembrane conductance regulator gene impacts bone formation. Am J Pathol 2012;180:2068–75.
[43] Paradis J, Wilke M, Haston CK. Osteopenia in Cftr-deltaF508 mice. J Cyst Fibros 2011;9:239–45.
[44] Rosenberg LA, Schluchter MD, Parlow AF, et al. Mouse as a model of growth retardation in cystic fibrosis. Pediatr Res 2006;59:191–5.
[45] Velard F, Delion M, Lemaire F, et al. Cystic fibrosis bone disease: is the CFTR corrector C18 an option for therapy? Eur Respir J 2015;45:845–8.
[46] Stalvey MS, Clines KL, Havasi V, et al. Osteoblast cftr inactivation reduces differentiation and osteoprotegerin expression in a mouse model of cystic fibrosis-related bone disease. PLoS ONE 2013;8:e80098.
[47] Stalvey MS, Havasi V, Tuggle KL, et al. Reduced bone length, growth plate thickness, bone content, and IGF-I as a model for poor growth in the CFTR-deficient rat. PLoS ONE 2017;12:e0188497.
[48] Le Henaff C, Hay E, Velard F, et al. Enhanced F508del-CFTR channel activity ameliorates bone pathology in murine cystic fibrosis. Am J Pathol 2014;184:1132–41.
[49] Maupin KA, Droscha CJ, Williams BO. A comprehensive overview of skeletal phenotypes associated with alterations in Wnt/beta-catenin signaling in humans and mice. Bone Res 2013;1:27–71.
[50] Croker SL, Reed W, Donlon D. Comparative cortical bone thickness between the long bones of humans and five common non-human mammal taxa. Forensic Sci Int 2016;260:e1–104.e17 104.
[51] Pankow S, Bamberger C, Calzolari D, et al. F508 CFTR interactome remodelling promotes rescue of cystic fibrosis. Nature 2015;528:510–16.
[52] Sun H, Wang Y, Zhang J, et al. CFTR mutation enhances dishevelled degradation and results in impairment of Wnt-dependent hematopoiesis. Cell Death Dis 2018;9:275.
[53] Le Henaff C, Mansouri R, Modrowski D, et al. Increased NF-kappaB activity and decreased Wnt/beta-Catenin signaling mediate reduced osteoblast differentiation and function in Deltaf508 cystic fibrosis transmembrane conductance regulator (CFTR) mice. J Biol Chem 2015;290:18009–17.
[54] Moverare-Skrtic S, Henning P, Liu X, et al. Osteoblast-derived WNT16 represses osteoclastogenesis and prevents cortical bone fragility fractures. Nat Med 2014;20:1279–88.